J Biomol NMR (2012) 52:141–150
DOI 10.1007/s10858-011-9588-z

ARTICLE

Sugar-to-base correlation in nucleic acids with a 5D APSY-HCNCH or two 3D APSY-HCN experiments

Barbara Krähenbühl · Daniela Hofmann · Christophe Maris · Gerhard Wider

Received: 31 August 2011 / Accepted: 16 November 2011 / Published online: 4 December 2011

Abstract A five-dimensional (5D) APSY (automated projection spectroscopy) HCNCH experiment is presented, which allows unambiguous correlation of sugar to base nuclei in nucleic acids. The pulse sequence uses multiple quantum (MQ) evolution which enables long constant-time evolution periods in all dimensions, an improvement that can also benefit non-APSY applications. Applied with an RNA with 23 nucleotides the 5D APSY-HCNCH experiment produced a complete and highly precise 5D chemical shift list within 1.5 h. Alternatively, and for molecules where the *out-and-stay* 5D experiment sensitivity is not sufficient, a set of *out-and-back* 3D APSY-HCN experiments is proposed: an intra-base (3D APSY-b-HCN) experiment in an MQ or in a TROSY version, and an MQ sugar-to-base (3D APSY-s-HCN) experiment. The two 3D peak lists require subsequent matching via the N1/9 chemical shift values to one 5D peak list. Optimization of the 3D APSY experiments for maximal precision in the N1/9 dimension allowed matching of all ^{15}N chemical shift values contained in both 3D peak lists. The precise 5D chemical shift correlation lists resulting from the 5D experiment or a pair of 3D experiments also provide a valuable basis for subsequent connection to chemical shifts derived with other experiments.

Keywords RNA · DNA · NMR · HCNCH · Projection spectroscopy · APSY · Sugar-to-base correlation · Automated assignment

Introduction

For the unambiguous resonance assignment of nucleic acids experiments play an important role which correlate the sugar nuclei H1′ and C1′ with the base nuclei C6/8 (pyrimidines/purines) and H6/8 (Fürtig et al. 2003; Flinders and Dieckmann 2006). Two main strategies are used: either the nuclei are correlated in one HCNCH experiment, or the relevant HC groups in sugar and base are correlated with the base N1/9 nuclei and connected via the N1/9 chemical shifts (HCN experiment). Several HCNCH- and HCN-type experiments have been proposed. Multiple quantum (MQ) sequences with selective inversion pulses (Fiala et al. 1998) have been shown to outperform single quantum (SQ) experiments (Sklenar et al. 1993a, b; Farmer et al. 1993, 1994; Tate et al. 1994) as well as MQ HCN experiments with non-selective pulses (Marino et al. 1997) or with spin-lock on protons (Sklenar et al. 1998); the latter experiment also used reduced dimensionality (Szyperski et al. 1993). Further modifications included transverse-relaxation optimized (TROSY) (Pervushin et al. 1998) experiments (Fiala et al. 2000; Riek et al. 2001), MQ bi-directional HCNCH experiments (Hu et al. 2001), a HC(N)C *out-and-back* experiment (Fürtig et al. 2004), a HCN-type sequence with combined TROSY and MQ effects (Brutscher and Simorre 2001), with additional resolution-enhancement and base-type-editing (Van Melckebeke et al. 2005), and with tailored correlation spectroscopy (Carlomagno and Fares 2006), as well as several versions for the determination of dipolar coupling constants (Yan et al. 2002; Jaroniec et al. 2005) or

Electronic supplementary material The online version of this article (doi:10.1007/s10858-011-9588-z) contains supplementary material, which is available to authorized users.

B. Krähenbühl · D. Hofmann · C. Maris · G. Wider (✉)
Institute of Molecular Biology and Biophysics, ETH Zurich, 8093 Zurich, Switzerland
e-mail: gsw@mol.biol.ethz.ch

torsion angles (Ravindranathan et al. 2003; Rinnenthal et al. 2007). In spite of this wide range of innovations, the experiments still suffer from limitations in sensitivity as a consequence of long ^{13}C–^{15}N transfer times, and in resolution due to small chemical shift dispersion. The latter impedes the result especially for the HCN methods, which are more sensitive than the HCNCH-type experiments, but rely on matching via only the N1/9 chemical shift.

The development of reduced dimensionality (Szyperski et al. 1993; Kim and Szyperski 2003) and projection spectroscopy methods (Kupce and Freeman 2003) opened also new perspectives for obtaining improved spectral resolution. In this context, automated projection spectroscopy (APSY) (Hiller et al. 2005, 2008b) has been established as a reliable method to provide precise chemical shift correlation lists of high dimensionality, which have successfully been used for automated resonance assignment in protein spectra (Fiorito et al. 2006; Hiller et al. 2008a; Narayanan et al. 2010; Gossert et al. 2011). In APSY, peak lists from a series of 2D projection spectra (Kupce and Freeman 2003) provide the input for the algorithm GAPRO (Hiller et al. 2005), which calculates the multidimensional peak list based on geometrical and statistical considerations.

In this publication we present a 5D APSY-HCNCH experiment and—as an alternative for larger nucleic acids—a procedure based on a pair of 3D APSY-HCN experiments. Measurements with an RNA stem-loop with 23 nucleotides provided complete and precise multidimensional peak lists. Based on these results the performance of the two APSY approaches in correlating sugar to base nuclei in nucleic acids will be discussed.

Materials and methods

Sample preparation

The nucleic acid used in this work was a 23 nucleotide long stem-loop RNA (SL23) with a molecular weight of 7.35 kDa. The uniformly [^{13}C, ^{15}N]-labeled RNA was transcribed in vitro using *in-house* produced T7 RNA polymerase containing a mutation (Pro266Leu) for improved efficiency (Guillerez et al. 2005). The respective DNA sequences of the T7 promotor (5′-TAATACGACTCACTA TAG-3′) and the designed template (5′-GGGACCTGGA AAGACCAGGTCCCTATAGTGAGTCGTATTA-3′) were purchased from Microsynth AG (Switzerland) and purified by anion-exchange HPLC in denaturing conditions (6 M urea at 85°C) (Allain et al. 2010). Urea and salts were removed by *n*-butanol extraction, and the purified oligonucleotides subsequently lyophilized. The [^{13}C, ^{15}N]-labeled NTPs (nucleoside triphosphates) were produced *in-house* from *E. coli* cells grown in [^{13}C, ^{15}N]-enriched M9 medium (Batey et al. 1992; Nyholm et al. 1995). The $MgCl_2$ concentration was optimized with respect to highest transcription yield at a fixed concentration of NTPs in 50 µl small-scale reactions. The large-scale reaction of 15 ml contained 20 mM $MgCl_2$, 6.4 mM [^{13}C, ^{15}N]-labeled NTPs, 1.2 µM template and T7 promotor (annealed at 70°C in equimolar ratio), 15 units pyrophosphate and 64 µg/ml T7 polymerase, and buffer conditions as described earlier (Price et al. 1998). The SL23 RNA was purified the same way as the DNA oligonucleotides. The final RNA preparation contained additional $n-1$, $n-2, n+1$ and $n+2$ products in minor concentrations that could not be separated chromatographically. The sample was dissolved in 250 µl D_2O with 10 mM phosphate buffer at pD 6.5, containing 0.2% NaN_3 and 1 mM EDTA; this solution was filled in a Shigemi tube (Shigemi Inc., Allison Park, PA, USA) for the NMR measurements. The RNA concentration was 1 mM, as determined by UV absorption measurement and PULCON (Wider and Dreier 2006).

Description of the pulse sequences

The sugar-to-base 5D APSY-HCNCH and the 3D APSY-HCN experiments are through-bond correlation experiments. Their coherence transfer pathways are illustrated for purines in Fig. 1. In the 5D APSY-HCNCH experiment, the coherence transfer starts on the sugar H1′, and passes over C1′, N1/9 and C6/8 to H6/8 of the base, where the signal is detected. The 3D APSY-HCN experiments are of the type *out-and-back*. All experiments are provided as a multiple quantum (MQ) version; the 3D APSY-b-HCN experiment in addition as a TROSY version for measurements at higher magnetic fields. The coherence pathways start with either the base H6/8 or the sugar H1′ and reach via the attached carbon N1/9, from where the path returns to the starting nucleus for detection.

The multiple quantum (MQ) pulse sequences of the 5D APSY-HCNCH and the 3D APSY-s-HCN experiments are shown in Fig. 2, and the sequences of the 3D APSY-b-HCN experiments in an MQ and a TROSY version in Fig. 3. The development of the 5D APSY-HCNCH was based on the MQ H(CNC)H sequence of Fiala et al. (1998). However, there are distinct differences which are on the one hand related to the inclusion of three additional evolution periods and on the other hand to optimizations which improve sensitivity and resolution. The initial step is a non-refocused INEPT transfer from H1′ to C1′ (Fig. 2a). H1′ and C1′ are then brought to a MQ state (double- and zero-quantum coherence). The MQ state is preserved during most of the C1′–N1/9 transfer period T_2. The H1′ evolution is performed in a constant-time manner (Bax and Freeman 1981) by shifting the off-resonance REBURP (Geen and Freeman 1991) pulse which selectively inverts H1′ at

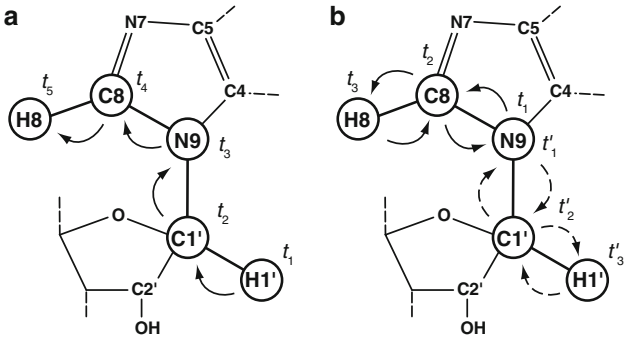

Fig. 1 Magnetization transfer pathway for purines **a** in the 5D APSY-HCNCH experiment, and **b** in the 3D APSY-HCN experiments with RNA. The pathway is equivalent to the one in conventional 2D and 3D HCNCH or HCN experiments (Sklenar et al. 1993a, b; Fiala et al. 2000; Riek et al. 2001). Evolution periods for frequency labeling were introduced for all nuclei along the coherence pathway. In (**a**), the INEPT coherence transfer steps are indicated by solid arrows. The resulting four indirect evolution periods are indicated by t_1 to t_4 and the acquisition time by t_5. In (**b**), the coherence transfer steps are indicated with dashed arrows for the HCN experiment starting on the sugar H1′ (3D APSY-s-HCN) and with solid arrows for the HCN experiment starting on the base H8 (3D APSY-b-HCN). The indirect evolution periods are indicated for the 3D APSY-b-HCN by t_1, t_2 and t_3, and for the 3D APSY-s-HCN by t_1', t_2' and t_3', where t_3 and t_3' are the direct acquisition periods. The transfer scheme is the same for pyrimidines, with the pyrimidine nuclei H6, C6 and N1 corresponding to the indicated purine nuclei H8, C8 and N9

5.5 ppm (pulse (*a*) in Fig. 2a) within the MQ period. The constant-time C1′ evolution period is implemented into the C1′–N1/9 transfer period with homonuclear carbon coupling evolution refocused by two cosine-modulated IBURP-2 (Geen and Freeman 1991) pulses (*c* in Fig. 2a) which selectively invert the frequency bands of C2′ as well as of C6/8. During T_3, N1/9 coherence anti-phase to C1′ is transformed into anti-phase coherence with respect to C6/8. The N1/9 evolution period is implemented during T_3 in a constant-time manner, the selective 180° pulse (*d* in Fig. 2a) that acts on C1′ and C6/8 is synchronized with the hard 180° pulse on ^{15}N. A cosine-modulated off-resonance IBURP-2 pulse (*e* in Fig. 2a) which inverts both C2 (pyrimidines) and C4/5/6 (purines) circumvents modulation of the signal by couplings to these nuclei during the N1/9 evolution period, and a 180° pulse on protons in the T_3 period refocuses evolution under the ^{15}N–^{1}H coupling Hamiltonian. The following T_5/T_6 time period is basically a "mirror image" of the elements during T_2; e.g. again the proton and carbon are mostly in a MQ state. Unlike during the T_2 period, the ^{15}N inversion pulse during T_5/T_6 (*f* in Fig. 2a) is a selective Q3 Gaussian (Emsley and Bodenhausen 1990) cascade on N1/9 in order to decouple C8 and H8 from N7 and avoid coherence losses; further, two REBURP pulses selectively invert H6/8 to refocus proton chemical shift evolution and reduce ^{1}H–^{15}N couplings (which are larger than the ^{1}H1′–^{15}N couplings). The two band-selective cosine-modulated IBURP-2 180° pulses (*e* in Fig. 2a) decouple C6/8 from C2 in pyrimidines as well as C4 and C6 in purines. The C6/8 constant-time evolution period is implemented by shifting all 180° pulses during T_5/T_6 synchronously. Finally, the period T_4 is a refocused INEPT transfer to generate in-phase coherence on H6/8, which is subsequently detected while ^{13}C and ^{15}N are decoupled. The carrier frequency on the proton channel was set to 4.7 ppm, in order to optimally suppress the signal of residual water with the first z-filter gradient.

The pulse schemes for the MQ APSY-HCN sequences (Figs. 2b, 3a) are to a large extent equivalent to the 2D MQ HCN sequences proposed earlier (Fiala et al. 1998). Differences include: an additional pair of gradients G_1 in the first INEPT element to suppress off-pathway coherences; a 180° ^{15}N-pulse in the ^{15}N evolution period t_1 in order to start evolution at 0 μs (Sklenar et al. 1998; Hiller et al. 2008b); implementation of the carbon evolution t_2 by shifting a hard 180° pulse on ^{13}C (instead of a selective pulse) with reduced amplitude and phases distortions and two IBURP-2 180° pulses (*h* and *e* in Figs. 2b, 3a, respectively) which refocus homonuclear carbon coupling evolution (see caption of Fig. 2); and finally the 180° REBURP pulses on ^{1}H (*a* and *b* in Figs. 2b, 3a, respectively) which refocus evolution of proton magnetization and long-range couplings between protons and carbons. For the 3D APSY-s-HCN experiment (Fig. 2b), the 180° pulse on ^{15}N in the second T_2 is non-selective. For the 3D APSY-b-HCN experiment (Fig. 3a), the 180° carbon pulse in the first T_2 transfer period is replaced with the same pulse triplet (selective—hard—selective) as in the carbon evolution period.

The TROSY version of the 3D APSY-b-HCN pulse sequence (Fig. 3b) is for the ^{13}C and the ^{15}N channels equivalent to the MQ sequence. The pulsing scheme on the ^{1}H channel corresponds to the one proposed earlier (Fiala et al. 2000), with protons along z and no inversion pulses during the C6/8–N1/9 transfer periods, and with two rectangular high-power 180° pulses placed symmetrically in the ^{15}N evolution period.

Data acquisition and processing

Most experiments were performed on a 500 MHz Bruker Avance III spectrometer equipped with a cryogenic ^{1}H/^{13}C/^{15}N triple resonance probe with z-gradient accessory. All spectra were measured on this spectrometer unless mentioned otherwise. Some additional measurements for an evaluation of the TROSY version were performed on a 900 MHz Bruker Avance I spectrometer with the same probe type. The 5D APSY-HCNCH experiment was measured with 16 projections within 1.5 h at 25 and 18°C. The spectral widths

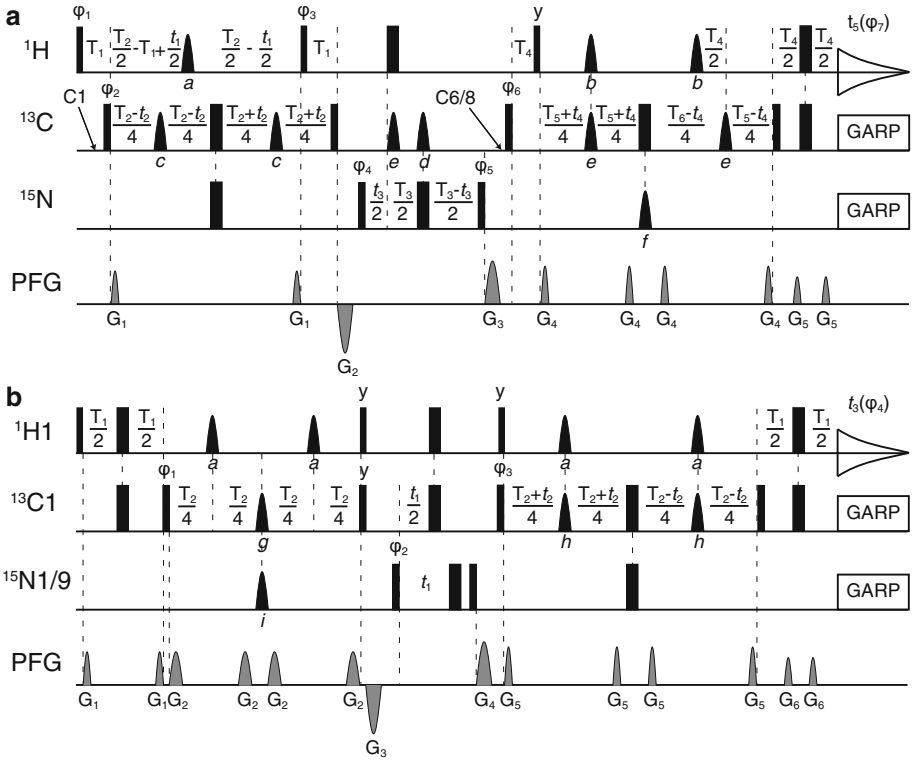

Fig. 2 Pulse sequences for through-bond correlations between sugar and base nuclei in RNA (Fig. 1): **a** 5D APSY-HCNCH and **b** 3D APSY-s-HCN. In (**a**), the carrier frequency is set to 4.7 ppm for ^{1}H, and to 160 ppm for ^{15}N; the ^{13}C carrier frequency is first set to 90.5 ppm corresponding to the chemical shift range of C1′ carbons (marked by the *arrow* labeled C1′), and later shifted to the base region at 139.5 ppm (*arrow* C6/8). Thin and wide black bars represent non-selective 90° and 180° high-power pulses. Black sine bell shapes labeled by the letters *a–f* indicate selective 180° pulses with specific excitation profiles; these selective pulses have the following properties (durations, excitation ranges and modulation frequencies are given for application on 500 MHz): (*a*) and (*b*) are off-resonance REBURP (Geen and Freeman 1991) pulses with a duration of 4,200 µs applied at (*a*) 5.5 ppm (H1′) and (*b*) 7.5 ppm (H6/8); (*c*), (*d*) and (*e*) are cosine-modulated IBURP-2 (Geen and Freeman 1991) pulses which selectively invert two spectral ranges simultaneously (*c*) inverts the chemical shift ranges 68 ± 8 ppm (C2′) and 138 ± 8 ppm (C6/8, in pyrimidine also partially C2 and C4) with a duration of 1,800 µs (*d*) inverts 90.5 ± 4.8 ppm (C1′) and 139.5 ± 4.8 ppm (C6/8) with a duration of 2,650 µs, and (*e*) 116 ± 5.5 ppm (purine C5) and 157 ± 5.5 ppm (pyrimidine C2, purine C4 and C6) with 2,450 µs. Thus, the three cosine modulation frequencies of the selective pulses (discussed in Sklenar et al. 1993a, 1998) correspond to 4,400, 3,080 and 2,580 Hz for (*c*), (*d*) and (*e*), respectively; (*f*) is a Q3 Gaussian cascade (Emsley and Bodenhausen 1990) with a duration of 700 µs. GARP (Shaka and Keeler 1987) decoupling sequences were applied during acquisition on ^{13}C with a field strength of 2.5 kHz and on ^{15}N with 1.39 kHz. The time periods T_i are $T_1 = 3.2$ ms, $T_2 = 40$ ms, $T_3 = 36.6$ ms, $T_4 = 2.5$ ms, $T_5 = T_6 - 2T_4$, $T_6 = 30$ ms. The phases of the pulses were set to *x*, unless indicated otherwise above the pulse symbol. The following phase cycle was applied: $\varphi_1 = 2(y), 2(-y)$; $\varphi_2 = 16(x), 16(-x)$; $\varphi_3 = 4(x), 4(-x)$; $\varphi_4 = x$; $\varphi_5 = x, -x$; $\varphi_6 = 8(x), 8(-x)$; receiver phase $\varphi_7 = \alpha, 2(-\alpha), \alpha, -\alpha, 2(\alpha), -\alpha$ with $\alpha = x, 2(-x), x$; φ_1 and φ_4 are exchanged for projections with ^{15}N evolution. Quadrature detection in the indirect dimensions was achieved by States-TPPI (Marion et al. 1989): φ_1 was incremented for the evolution period t_1 (H1′), φ_2 for t_2 (C1′), φ_4 for t_3 (N1/9), and φ_6 for t_4 (C6/8). The sine-bell shaped gradient pulses (PFG) were applied along the *z*-axis with the following durations and strengths: G_1: 500 µs, 12 G/cm; G_2: 1,000 µs, −35 G/cm; G_3: 1,000 µs, 20 G/cm; G_4: 500 µs, 16 G/cm; G_5: 500 µs, 7 G/cm. **b** 3D APSY-s-HCN pulse sequence with the same experimental details as described in (**a**) except that the ^{13}C offset was set to 90.5 ppm; (*g*) is an on-resonance (C1′) REBURP pulse with duration 2,800 µs (*h*) is an off-resonance IBURP-2 pulse at 70 ppm (C2′) with duration 1,800 µs, and (*i*) an on-resonance (N1/9) REBURP pulse with duration 1,800 µs; time periods $T_1 = 3.0$ ms and $T_2 = 32$ ms; phase cycle: $\varphi_1 = 4(x), 4(-x)$; $\varphi_2 = x, -x$; $\varphi_3 = 2(y), 2(-y)$; receiver phase $\varphi_4 = \alpha, 2(-\alpha), \alpha, -\alpha, 2(\alpha), -\alpha$ with $\alpha = x, 2(-x), x$. States-TPPI quadrature detection in the indirect dimensions was achieved by incrementing φ_2 for t_1 (^{15}N), and φ_3 for t_2 (^{13}C). PFGs were applied with the following durations and strengths: G_1: 500 µs, 5 G/cm; G_2: 1,000 µs, 6 G/cm; G_3: 1,000 µs, −35 G/cm; G_4: 1,000 µs, 20 G/cm; G_5: 500 µs, 16 G/cm; G_6: 500 µs, 7 G/cm

were set to 1,700, 1,132, 1,774, 1,384 and 8,503 Hz, and the maximal acquisition times in the projection spectra to 34.1, 33.6, 33.8, 16.9 and 120.5 ms for H1′, C1′, N1/9, C6/8 and H6/8 (aq), respectively. For the 3D APSY-s-HCN experiment, 32 projections were measured within 1.4 h at 25°C, with the spectral widths set to 1,774, 1,132 and 6,010 Hz, and the maximal acquisition times to 56.4, 19.4 and 120.5 ms for N1/9, C1′ and H1′ (aq), respectively. For the b-HCN, 22 projections were measured within 43 min at 25°C, with the spectral widths set to 1,774, 1,132 and 6,010 Hz (multiplied

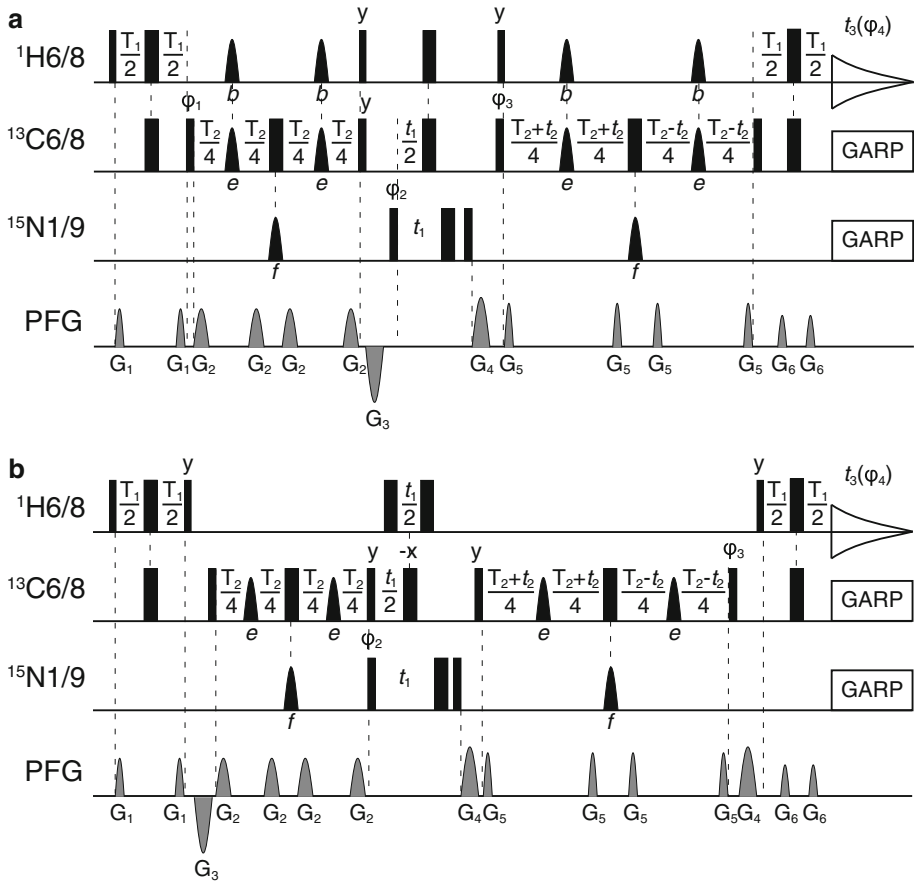

Fig. 3 Pulse sequences for an MQ **a** and a TROSY **b** version of an intra-base 3D APSY-b-HCN experiment. The experimental details of the two pulse sequences are largely equivalent to those described in Fig. 2, including the shaped pulses (*b*), (*e*) and (*f*), the quadrature detection scheme (as in Fig. 2b) and the gradient pulses. The ^{13}C offset was set to 139.5 ppm, and the time periods to $T_1 = 2.5$ ms and $T_2 = 30$ ms. The MQ sequence (**a**) uses the same phase cycling as the MQ sugar-to-base sequence (Fig. 2b). The TROSY sequence (**b**) employs a slightly modified version with $\varphi_2 = x, -x$; $\varphi_3 = 2(x), 2(-x)$; receiver phase $\varphi_4 = x, 2(-x), x$

with a factor of 9/5 for measurements at 900 MHz), and the maximal acquisition times to 44.6, 20.2 and 120.5 ms for N1/9, C6/8 and H6/8 (aq), respectively. Complete parameter sets can be found in the Supplementary Material.

The projection experiments were set up from a parent data set with a macro script ("AU" program) using the spectrometer software Topspin 2.1 (Bruker, Karlsruhe, Germany). Automated serial processing with automatically generated input files was performed with Prosa 6.4 (Güntert et al. 1992). A more detailed description of the procedures for measurement and processing of the experiments is provided in the Supplementary Material.

Analysis

The projection spectra were automatically peak picked by GAPRO 0.98 (Hiller et al. 2005), which then calculated a 5D peak list for the 5D APSY-HCNCH experiment and two separate 3D peak lists for the 3D APSY-HCN experiments. The two 3D chemical shift correlation lists were merged into one 5D peak list by a software routine written in MATLAB (R2010b, The MathWorks, Natick, MA, USA). Each ^{15}N chemical shift in the lists was matched to the nearest neighbor in the other 3D HCN list providing a 5D peak list (see Supplementary Material for more details).

Results and discussion

A sugar-to-base 5D APSY-HCNCH experiment and a method combining a sugar-to-base and an intra-base 3D APSY-HCN experiment are presented. Both approaches allow automated correlation of sugar to base resonances in nucleic acids.

For the 5D APSY-HCNCH experiment, the GAPRO analysis of 16 projection spectra of SL23 measured within 1.5 h at 25°C on a 500 MHz spectrometer resulted in a complete and precise 5D chemical shift correlation list. The pulse sequence refinement led to significantly improved sensitivity also independent of its use as an APSY experiment, which is mostly based on the new H1′ evolution. The signal-to-noise ratio of the peaks in the 2D H1′-H6/8 spectrum measured with our sequence is on average 80% higher than with the previous incremented H1′ evolution (Fiala et al. 1998). The improvement is partially a result of the modified pulsing scheme with an MQ ^{1}H–^{13}C transfer and the three-pulse-element on ^{13}C described above, but mainly the possibility to use the full C1′–N1/9 transfer period—with H1′–C1′ in MQ state—for a constant-time H1′ evolution of up to 34 ms resulting in significantly narrower line widths. When used as a 5D APSY experiment, the high dimensionality and the high

resolution in the projection spectra due to exploited constant-time evolutions allowed distinguishing peaks which are strongly overlapping in conventional experiments. For a comparable spectral resolution, the acquisition of a classical HCNCH experiment with only three dimensions would take 2–8 times longer than the full 5D APSY experiment depending on the choice of nuclei in the indirect dimensions, and still be prone to overlap due to the lower dimensionality. Moreover, the APSY chemical shift precision could not be reached even for separated peaks, since APSY benefits in addition to the spectral resolution from averaging of the values from several projection spectra. The fraction of time domain data points measured in all projections compared to a corresponding classical 5D HCNCH experiment is only 0.0039%, notably without violating the Nyquist theorem, and therewith artifact-free; classical acquisition of the 5D experiment would require several years of measurement time. If 4 dimensions are expected to be sufficient for full separation, the experiment can be run as a 4D APSY which approximately halves the measurement time with respect to the 5D APSY; e.g. the analysis of the nine projection spectra without N1/9 (4D APSY-HC(N)CH) which were measured within 43 min led to a complete and precise 4D peak list (H1′–C1′–C6/8–H6/8). A further 5D APSY-HCNCH data set with identical parameters was measured at 18°C, and served to estimate the performance at somewhat higher correlation times, and hence for potential applications on larger nucleic acids. The sensitivity was still sufficient to result in a 5D correlation list for all nucleotides except G1, for which conformational exchange effects are more pronounced at 18°C.

For applications which require even higher sensitivity, a method with two 3D APSY-HCN experiments is presented as an alternative. These *out-and-back* experiments exhibit shorter total transfer times, and thus provide higher sensitivity than the *out-and-stay* HCNCH experiment. The respective relative sensitivity in the intra-base experiment is for the MQ and the TROSY version spectrometer field dependent. The sensitivity differences were estimated by comparing the intensity in spectra obtained from the first FIDs of the multi-dimensional experiments: With this measure the MQ version of the 3D APSY-b-HCN has an approximate relative sensitivity with respect to the HCNCH of 1.5, and the 3D APSY-s-HCN experiment of 4. The lower sensitivity of the MQ version of 3D APSY-b-HCN compared to the 3D APSY-s-HCN can be explained with the larger chemical shift anisotropy (CSA) (Fiala et al. 2000) in the base and consequential relaxation, and with the more complex scalar coupling network which cannot be fully decoupled. On the other hand, the 3D APSY-s-HCN experiment requires a higher number of projections due to the lower dispersion of the H1′ and C1′ signals in comparison to the H6/8 and C6/8 signals. The combination of the two 3D HCN peak lists to a 5D sugar-to-base HCNCH peak list by matching via only the N1/9 chemical shifts requires an exceptionally high precision in this dimension. Hence, the two 3D APSY-HCN experiments need to be acquired with a higher number of projections compared to the 5D APSY-HCNCH, and with an optimized set of projection angles; the method can therefore outperform the 5D experiment only for nucleic acids, for which the sensitivity in the latter is not sufficient.

Corresponding N1/9-precision-optimized data sets of two 3D APSY-HCN experiments were measured with SL23. The processing and analysis of the 20 2D projections of a 3D APSY-b-HCN data set measured within 43 min led to a complete and artifact free peak list; the 32 projections of the 3D APSY-s-HCN data set measured within 1.4 h led to precise chemical shift values for 21 out of 23 multidimensional peaks. Only average chemical shift values were found for C16 and C6, since the difference between their respective chemical shifts was smaller than the spectral resolution in all 3D APSY-s-HCN dimensions; the same problem does not occur in the 5D experiment due to superior separation. Both 3D peak lists were devoid of artifacts, but contained as a consequence of the SL23 3′-end heterogeneity (see Sample preparation) some additional correlation frequencies (P1–P4 in Fig. 4), which were unambiguously distinguishable from the peaks of interest. The resonances of the 21 nucleotides found in both experiments could be unambiguously merged to 5D correlations (Fig. 4). Even in highly overlapping spectral regions, e.g. around 169.13 ppm, where the N1/9 chemical shifts of G1, G3, G9 and G18 "cluster" within ±0.03 ppm with the closest ones being separated by 0.01 ppm, the precision of the APSY peak lists provided unambiguous matching.

The APSY experiments exploit the same magnetization transfer pathway (Fig. 1) as previous HCNCH and HCN experiments (Fiala et al. 1998). Differences in the pulse scheme compared to these conventional MQ sequences have been described in "Materials and methods". Still, there are some features which need additional consideration. In the 5D APSY-HCNCH pulse sequence, the use of only one selective 180° pulse on H1′ during the H1′–C6/8–N1/9 transfer period allowed the combination of the H1′ evolution period and the transfer period into a constant-time evolution of up to 34 ms instead of a progressively increasing evolution time in addition to the transfer period as proposed by (Fiala et al. 1998, 2000). As in their sequence, H1′–H2′ scalar coupling is active during t_1; with a value of 1–3 Hz in the C3′-*endo* conformation it can be neglected (Fiala et al. 1998). The small long-range couplings of H1′ to carbons and of C1′ to protons during the respective evolution periods can usually also be neglected. During T_5/T_6 (Fig. 2a), the application of the

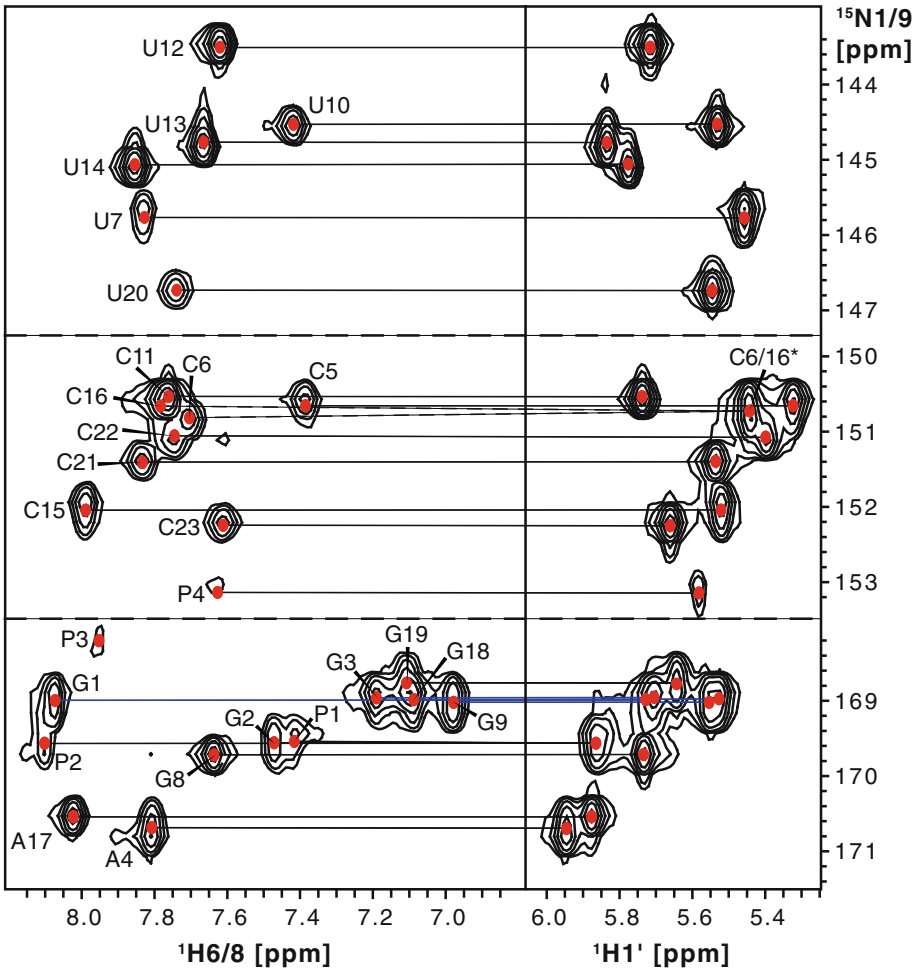

Fig. 4 Three parts of the N1/9–H6/8 projection spectrum of a 3D APSY-b-HCN (on the *left*) and three parts of the N1/9–H1′ projection spectra a 3D APSY-s-HCN (on the *right*) of a 23-nucleotide stem loop RNA (SL23). The positions of the multidimensional peak list calculated from the complete set of 3D APSY-HCN projections are marked with red dots. The horizontal lines indicate the merging of the two 3D peak lists via the N1/9 dimension. The lines which indicate the matching for G1, G3, G9 and G18 are highlighted in blue: the N1/9 chemical shifts of these guanines lie within 0.06 ppm, but their precision (average chemical shift deviation <0.0047 ppm or 0.24 Hz for matched N1/9) still allows unambiguous matching. Assignments are indicated with one-letter symbols and the RNA sequence number of the corresponding nucleic acid. Peaks *P1–P4* originate from truncated RNAs. For the cytosines C6 and C16, the cross peaks could not be separated in the 3D APSY-s-HCN experiment (marked as C6/16*) due to almost identical chemical shift values in all three dimensions. Thus, N1 matching was incomplete for cytosines in the 3D approach, but was obtained in the 5D experiment

three-pulse element (similar as in Van Melckebeke et al. 2005) for carbon inversion/decoupling in the base region has shown to lead to slightly more signal also independent from C6/8 evolution, on the one hand due to decoupled long-range heteronuclear H6/8–carbon, H6/8–N1/9 and C6/8-proton couplings, on the other hand due to improved combined inversion profiles. The long-range coupling of H6/8 to pyrimidine C2, and purine C4, C5 and C6 (all carbons affected by pulse *e* in Fig. 2a) modulates the signal during t_4 for projections with active C6/8 evolution; since the corresponding coupling constants are usually smaller than 5 Hz, this effect does not reduce the sensitivity noticeably.

The changes for the 3D APSY-HCN sugar-to-base (Fig. 2b) and the MQ version of the intra-base (Fig. 3a) experiment in comparison to the conventional sequences (Fiala et al. 1998) are less extensive than for the HCNCH experiment. A ^{13}C evolution period had to be added which is achieved by using the same three-pulse-element for carbon inversion as described for the HCNCH sequence. The same element is also applied within the first T_2 part of the 3D HCN-b-APSY experiment due to the previously mentioned better selection properties in the base region.

The 5D APSY-HCNCH and the 3D APSY-s-HCN pulse sequences presented here do not include TROSY elements. Existing TROSY versions of both experiments proved not to be advantageous (Fiala et al. 2000). Only for intra-base experiment it could be shown by comparing 2D ^{1}H–^{15}N cross peak intensities of TROSY and MQ spectra that TROSY provides a benefit, particularly at high magnetic

fields (Fiala et al. 2000; Riek et al. 2001; Brutscher and Simorre 2001). Comparisons of the intra-base TROSY and MQ experiments were performed at 500 MHz and at 900 MHz. The reported sensitivity enhancement by TROSY of a factor of ~1–3 at 500 MHz and of ~3–9 at 900 MHz could approximately be confirmed. However, the inclusion of an appropriate C6/8 evolution proved to be a challenge: in earlier TROSY versions there is either no ^{13}C evolution included (Fiala et al. 2000), or one without ^{13}C and ^{15}N decoupling which limits evolution to 4 ms (Riek et al. 2001), or one with ^{13}C–^{15}N in MQ state enabling a C6/8 evolution of up to 60 ms (Brutscher and Simorre 2001), but with significantly impeded ^{15}N evolution (<15 ms). We present here (Fig. 3b) a pulse sequence which combines TROSY with the same favorable ^{13}C pulsing elements during evolution and ^{13}C–^{15}N transfers as in our intra-base MQ sequence (Fig. 3a). The often more sensitive TROSY version has some potential drawbacks with respect to the MQ sequence. There is no explicit spin-state selection, therefore the second doublet peak can appear in the spectrum depending on its relaxation properties and on the relative proton and carbon steady-state contributions (Brutscher and Simorre 2001); explicit selection would prolong the sequence and hence reduce the sensitivity. Further, the C6/8 peaks in the TROSY experiment are shifted by $J_{CH}/2$ making the correlation with non-TROSY peak lists less precise. At lower magnetic fields (up to ~600 MHz), where the sensitivity range of the weakest signals is comparable for the two approaches, and the probability for visible doublet peaks in the TROSY version is high, we recommend to use the MQ version of the experiment. At higher fields the TROSY version benefits from improved spin-state selectivity, whereas the MQ state suffers from increased relaxation by CSA, which makes TROSY the method of choice for the intra-base HCN experiment. The overall performance of the experiments was in general better at 500 MHz than at 900 MHz, it is therefore recommended to use lower fields unless required otherwise by experimental procedures. As generally valid for APSY experiments, the presented pulse sequences can readily be used as classical 2D versions with acquisition on H6/8 and correlation to H1′, C1′, N1/9, or C6/8, or as APSY versions with three to five dimensions. The number and type of nuclei to be included in the final peak list can therefore be tailored to specific requirements.

The precision in the final peak lists was estimated based on the average deviations between the chemical shift values from the 5D and the 3D peak lists for the same nuclei which were normalized with the average differences between the values. The resulting average deviations were 0.002 ppm for H1′, 0.009 ppm for C1′, 0.023 ppm for N1/9, and 0.009 ppm for C6/8; considering the gyromagnetic ratios of the nuclei, the deviations lie all in the same range of 1.1 Hz. The average chemical shift deviation of the corresponding N1/9 values from the precision-optimized 3D APSY-HCN experiments was 0.0047 ppm (0.24 Hz).

The experiments applied here to RNA can also be used with DNA molecules; their applicability is, however, conformation-dependent, as discussed in detail earlier (Fiala et al. 1998). The APSY results were successfully verified by comparing the resulting chemical shift values and correlations to a manual assignment of the SL23 RNA with classical experiments. These assignments were also used for the discussion of the results. Additional APSY experiments could correlate further sugar, base and backbone nuclei and provide the basis for automated assignment strategies. The present HCNCH methods serve as a first—and crucial—building block of such an approach for nucleic acids.

Conclusions

Two approaches based on APSY are presented that both provide reliable intra-nucleotide sugar-to-base correlations with a uniformly [^{13}C, ^{15}N]-labeled nucleic acid sample. The 5D APSY-HCNCH experiment provided a precise and complete chemical shift correlation list for an RNA stem-loop with 23 nucleotides within 1.5 h. The high dimensionality of the experiment and the feasibility of very long indirect constant-time evolutions during the coherence transfer periods in the projection spectra minimize potential spectral overlap, and lead along with APSY-specific statistical selection and averaging effects to high precision (~1.1 Hz) and accuracy of the final peak list. The optimized HCNCH pulse sequence can also be run as a conventional 2D experiment, or as a 3D or 4D APSY with the desired choice of indirect dimensions; e.g. a 2D H1′-H6/8 version in our hands demonstrated a 80% higher sensitivity than the best previous HCNCH experiments. An alternative approach for larger nucleic acids with two *out-and-back* 3D APSY-HCN spectra provides higher sensitivity, but at the cost of an increased probability for spectral overlap. The subsequent matching of the two resulting peak lists via the N1/9 chemical shifts is for conventional experiments often impeded by the small dispersion of the resonances and consequent ambiguities. The significantly higher precision of the chemical shifts obtained from the 3D APSY-HCN experiments (~0.24 Hz for N1/9) considerably relieves this situation.

Acknowledgments We thank Prof. Sebastian Hiller (University Basel) for technical discussions, and Prof. Frédéric Allain (ETH Zurich) for the provision of [^{13}C, ^{15}N]-labeled nucleotides. The Swiss National Fund (SNF) is gratefully acknowledged for financial support (project 200021_120048).

References

Allain FHT, Duss O, Maris C, von Schroetter C (2010) A fast, efficient and sequence-independent method for flexible multiple segmental isotope labeling of RNA using ribozyme and RNase H cleavage. Nucleic Acids Res 38(20). doi:10.1093/nar/gkq756

Batey RT, Inada M, Kujawinski E, Puglisi JD, Williamson JR (1992) Preparation of isotopically labeled ribonucleotides for multidimensional NMR spectroscopy of RNA. Nucleic Acids Res 20(17):4515–4523

Bax A, Freeman R (1981) Investigation of complex networks of spin–spin coupling by two-dimensional NMR. J Magn Reson 44(3):542–561

Brutscher B, Simorre JP (2001) Transverse relaxation optimized HCN experiment for nucleic acids: combining the advantages of TROSY and MQ spin evolution. J Biomol NMR 21(4):367–372

Carlomagno T, Fares C (2006) SHARP-TACSY: triple-band tailored correlated spectroscopy for base-to-sugar transfer in nucleic acid residues with intermediate time scale motions. J Am Chem Soc 128(30):9856–9862

Emsley L, Bodenhausen G (1990) Gaussian pulse cascades—new analytical functions for rectangular selective inversion and in-phase excitation in NMR. Chem Phys Lett 165(6):469–476

Farmer BT, Müller L, Nikonowicz EP, Pardi A (1993) Unambiguous resonance assignments in ^{13}C, ^{15}N-labeled nucleic acids by 3D triple resonance NMR. J Am Chem Soc 115(23):11040–11041

Farmer BT, Müller L, Nikonowicz EP, Pardi A (1994) Unambiguous through-bond sugar-to-base correlations for purines in ^{13}C, ^{15}N-labeled nucleic acids—the $H_sC_sN_b$, $H_sC_s(N)_bC_b$, and $H_bN_bC_b$ experiments. J Biomol NMR 4(1):129–133

Fiala R, Jiang F, Sklenai V (1998) Sensitivity optimized HCN and HCNCH experiments for ^{13}C/^{15}N labeled oligonucleotides. J Biomol NMR 12(3):373–383

Fiala R, Czernek J, Sklenar V (2000) Transverse relaxation optimized triple-resonance NMR experiments for nucleic acids. J Biomol NMR 16(4):291–302

Fiorito F, Hiller S, Wider G, Wüthrich K (2006) Automated resonance assignment of proteins: 6D APSY-NMR. J Biomol NMR 35(1):27–37

Flinders J, Dieckmann T (2006) NMR spectroscopy of ribonucleic acids. Prog Nucl Mag Res Sp 48(2–3):137–159

Fürtig B, Richter C, Wöhnert J, Schwalbe H (2003) NMR spectroscopy of RNA. Chembiochem 4(10):936–962

Fürtig B, Richter C, Bermel W, Schwalbe H (2004) New NMR experiments for RNA nucleobase resonance assignment and chemical shift analysis of an RNA UUCG tetraloop. J Biomol NMR 28(1):69–79

Geen H, Freeman R (1991) Band-selective radiofrequency pulses. J Magn Reson 93(1):93–141

Gossert AD, Hiller S, Fernandez C (2011) Automated NMR resonance assignment of large proteins for protein-ligand interaction studies. J Am Chem Soc 133(2):210–213

Guillerez J, Lopez PJ, Proux F, Launay H, Dreyfus M (2005) A mutation in T7 RNA polymerase that facilitates promoter clearance. Proc Natl Acad Sci USA 102(17):5958–5963

Güntert P, Dötsch V, Wider G, Wüthrich K (1992) Processing of multidimensional NMR data with the new software PROSA. J Biomol NMR 2(6):619–629

Hiller S, Fiorito F, Wüthrich K, Wider G (2005) Automated projection spectroscopy (APSY). Proc Natl Acad Sci USA 102(31):10876–10881

Hiller S, Joss R, Wider G (2008a) Automated NMR assignment of protein side chain resonances using automated projection spectroscopy (APSY). J Am Chem Soc 130(36):12073–12079

Hiller S, Wider G, Wüthrich K (2008b) APSY-NMR with proteins: practical aspects and backbone assignment. J Biomol NMR 42(3):179–195

Hu WD, Gosser YQ, Xu WJ, Patel DJ (2001) Novel 2D and 3D multiple-quantum bi-directional HCNCH experiments for the correlation of ribose and base protons/carbons in ^{13}C/^{15}N labeled RNA. J Biomol NMR 20(2):167–172

Jaroniec CP, Boisbouvier J, Tworowska I, Nikonowicz EP, Bax A (2005) Accurate measurement of ^{15}N–^{13}C residual dipolar couplings in nucleic acids. J Biomol NMR 31(3):231–241

Kim S, Szyperski T (2003) GFT NMR, a new approach to rapidly obtain precise high-dimensional NMR spectral information. J Am Chem Soc 125(5):1385–1393

Kupce E, Freeman R (2003) Projection-reconstruction of three-dimensional NMR spectra. J Am Chem Soc 125(46):13958–13959

Marino JP, Diener JL, Moore PB, Griesinger C (1997) Multiple-quantum coherence dramatically enhances the sensitivity of CH and CH_2 correlations in uniformly ^{13}C-labeled RNA. J Am Chem Soc 119(31):7361–7366

Marion D, Ikura M, Tschudin R, Bax A (1989) Rapid recording of 2D NMR spectra withoug phase cycling—application to the study of hydrogen-exchange in proteins. J Magn Reson 85(2):393–399

Narayanan RL, Dürr UHN, Bibow S, Biernat J, Mandelkow E, Zweckstetter M (2010) Automatic assignment of the intrinsically disordered protein Tau with 441-residues. J Am Chem Soc 132(34):11906–11907

Nyholm T, Andang M, Hotchkiss G, Hard T, Baumann H, Larsson S, Ahrlundrichter L (1995) A method for production of ^{13}C/^{15}N double-labeled RNA in *Escherichia Coli*, and subsequent in vitro synthesis of ribonucleotide 5′-triphosphates. J Biochem Biophys Methods 30(1):59–68

Pervushin KV, Wider G, Wüthrich K (1998) Single transition-to-single transition polarization transfer (ST2-PT) in ^{15}N, ^{1}H-TROSY. J Biomol NMR 12(2):345–348

Price SR, Oubridge C, Varani G, Nagai K (1998) Preparation of RNA:protein complexes for X-ray crystallography and NMR. In: Smith CWJ (ed) RNA-protein interactions: a practical approach, vol 192. Oxford University Press, Oxford, pp 37–74

Ravindranathan S, Kim CH, Bodenhausen G (2003) Cross correlations between ^{13}C–^{1}H dipolar interactions and ^{15}N chemical shift anisotropy in nucleic acids. J Biomol NMR 27(4):365–375

Riek R, Pervushin K, Fernandez C, Kainosho M, Wüthrich K (2001) ^{13}C, ^{13}C- and ^{13}C, ^{1}H-TROSY in a triple resonance experiment for ribose-base and intrabase correlations in nucleic acids. J Am Chem Soc 123(4):658–664

Rinnenthal J, Richter C, Ferner J, Duchardt E, Schwalbe H (2007) Quantitative Gamma-HCNCH: determination of the glycosidic torsion angle chi in RNA oligonucleotides from the analysis of CH dipolar cross-correlated relaxation by solution NMR spectroscopy. J Biomol NMR 39(1):17–29

Shaka AJ, Keeler J (1987) Broadband spin decoupling in isotropic liquids. Prog Nucl Mag Res Sp 19:47–129

Sklenar V, Peterson RD, Rejante MR, Feigon J (1993a) 2D and 3D HCN experiments for correlating base and sugar resonances in ^{15}N, ^{13}C-labeled RNA oligonucleotides. J Biomol NMR 3(6):721–727

Sklenar V, Peterson RD, Rejante MR, Wang E, Feigon J (1993b) 2D triple-resonance HCNCH experiment for direct correlation of ribose H1′ and base H6/8 protons in ^{13}C, ^{15}N-labeled RNA oligonucleotides. J Am Chem Soc 115(25):12181–12182

Sklenar V, Dieckmann T, Butcher SE, Feigon J (1998) Optimization of triple-resonance HCN experiments for application to larger RNA oligonucleotides. J Magn Reson 130(1):119–124

Szyperski T, Wider G, Bushweller JH, Wüthrich K (1993) Reduced dimensionality in triple-resonance NMR experiments. J Am Chem Soc 115(20):9307–9308

Tate S, Ono A, Kainosho M (1994) An alternative triple-resonance method for the through-bond correlation of intranucleotide H1′ and H8 NMR signals of purine nucleotides. Application to a DNA dodecamer with fully ^{13}C, ^{15}N-labeled deoxyadenosine residues. J Am Chem Soc 116(13):5977–5978

Van Melckebeke H, Pardi A, Boisbouvier J, Simorre JP, Brutscher B (2005) Resolution-enhanced base-type-edited HCN experiment for RNA. J Biomol NMR 32(4):263–271

Wider G, Dreier L (2006) Measuring protein concentrations by NMR spectroscopy. J Am Chem Soc 128:2571–2576

Yan JL, Corpora T, Pradhan P, Bushweller JH (2002) MQ-HCN-based pulse sequences for the measurement of ^{13}C1′–^{1}H1′, ^{13}C1′–^{15}N, ^{1}H1′–^{15}N, ^{13}C1′–^{13}C2′, ^{1}H1′–^{13}C2′, ^{13}C6/8–^{1}H6/8, ^{13}C6/8–^{15}N, ^{1}H6/8–^{15}N, ^{13}C6–^{13}C5, ^{1}H6–^{13}C5 dipolar couplings in ^{13}C, ^{15}N-labeled DNA (and RNA). J Biomol NMR 22(1):9–20